

# ON THE DETERMINATION OF THE PHOTOSPHERIC VELOCITY DISTRIBUTION FROM PROFILES OF WEAK FRAUNHOFER LINES

R. J. RUTTEN, P. HOYNG, and C. DE JAGER

*The Astronomical Institute at Utrecht, The Netherlands*

(Received 22 May, 1974)

**Abstract.** We derive the conditions under which the profile of a weak Fraunhofer line can be described as the convolution of the separate profiles of damping, thermal and non-thermal motions at the average depth of formation of the line. The average velocity distribution along the line of sight, rather than its customary chosen macro- and micro-turbulent components, is then found from the deconvolution of the observed profile with the known other contributions. Reversely, the observed profiles can be compared to predicted profiles on the basis of De Jager's (1974) theoretical turbulence broadening curves.

These two methods are tested on four suitable lines. The results indicate a non-gaussian velocity distribution with a rms velocity of about  $3 \text{ km s}^{-1}$  and show that the photospheric turbulence is not incompatible with Kolmogoroff's law.

## 1. Introduction

The photospheric motion field is usually described by its *macroturbulent* and *micro-turbulent* components that measure the motions of 'large' and of 'small' elements as experienced by a photon. An infinitesimally narrow Fraunhofer line, instantaneously observed at one mathematical point on the solar disc, would be displaced by macro-turbulence and broadened by micro-turbulence, respectively measured by the second and first moment of the profile (De Jager, 1972).

This description is physically realistic only when all non-thermal motions are indeed either macroturbulent or micro-turbulent. In general, however, one must introduce the concept of a 'spectrum of turbulence': i.e., the Fourier decomposition of all motions along the line of sight; in this connection a wavelength  $l$  and a wavenumber  $k = 2\pi/l$  are introduced. The one-dimensional spectrum of turbulence is the distribution of the turbulent energy  $\frac{1}{2}\langle v_k^2 \rangle$  contained in the motion components with wavenumbers between  $k$  and  $k + dk$ , with  $\langle v_k^2 \rangle$  the average over their velocity distribution. Following De Jager (1972), the distinction between macroturbulence and micro-turbulence is then found by means of the 'optical scale height'  $\theta = dz/d \log \tau$  where  $\tau$  is the continuous optical depth and  $z$  the geometrical depth. The mean free path of a photon at the level  $\tau = 1$  is about  $\theta$ . Macroturbulent motions have  $k\theta \ll 1$ ; micro-turbulent motions have  $k\theta \gg 1$ . This distinction loses part of its significance when the wavenumbers with  $k\theta \approx 1$  contain a significant part of the turbulent energy. In fact, there are indications that the greater part of the photospheric turbulent energy is contained in wavenumbers with  $k\theta \approx 1$  (De Jager, 1972). The derivation of the turbulence spectrum as a whole is therefore to be preferred.

There are two aspects of the turbulence spectrum to be studied: the distribution of turbulent energy over the wavenumbers and the distribution function of the velocities. In this paper we are interested in the second aspect: we discuss the extraction of the velocity distribution of all non-thermal motions from observations of weak Fraunhofer lines. In Section 2 we obtain a general expression for the profile of a weak line that is affected by a non-thermal motion field, averaged over a large area of the solar disc. This expression is non-linear; we derive the conditions under which it is simplified to a linear convolution integral that can be solved numerically. As an example we apply the method in Section 3 to 4 suitable Fraunhofer lines; the results are discussed in Section 4. Finally we compare these four line profiles with the turbulent broadening predicted by de Jager (1974).

## 2. The Profile of a Weak Line Affected by a Motion Field

### 2.1. THE 'TRUE' PROFILE

We start to derive the profile of a weak line observed instantaneously at a mathematical point on the solar disc. Assume that the line-of-sight component of the non-thermal motion field in the solar atmosphere (depth coordinate  $z$ ) is given by  $\Phi(x, y, z, t)$ .

The absorption coefficient at a depth  $z$  has its maximum value at a wavelength distance from the unshifted line center  $\lambda_0$

$$\lambda_c(z) - \lambda_0 = \frac{\lambda_0}{c} \Phi(z). \quad (1)$$

Functional dependences on  $x$ ,  $y$  and  $t$  are not given explicitly. The influence of thermal motions and damping is to broaden the line into a Voigt profile. Hence, defining  $\Delta\lambda = \lambda - \lambda_0$ , the line absorption coefficient  $\kappa_l$  at a depth  $z$  is given by

$$\kappa_l(\Delta\lambda, z) = \frac{\kappa(z)}{\delta\sqrt{\pi}} H\left(\frac{\gamma}{2\Delta\omega_D}, \frac{\Delta\lambda - \lambda_0\Phi(z)/c}{\delta}\right), \quad (2)$$

where

$$\Delta\omega_D = \frac{2\pi c}{\lambda^2} \Delta\lambda_D \equiv \frac{2\pi c}{\lambda^2} \delta.$$

Here,  $\delta = \lambda(2RT/\mu)^{1/2}/c$  is the thermal Doppler width,  $\gamma$  is the damping constant,  $\kappa(z)$  is the total line absorption coefficient and  $H(\alpha, v)$  is the Voigt function (Unsöld, 1955, p. 261). Since we are dealing with weak lines, the relative line depression  $r(\Delta\lambda)$  is given by (cf. Unsöld, 1955, p. 385)

$$r(\Delta\lambda) = \int_0^\infty d\tau_\lambda \frac{\kappa_l}{\kappa_\lambda} g_1(\tau_\lambda), \quad (3)$$

where  $g_1(\tau_\lambda)$  is the weighting function, specific for a given atmospheric model (cf.

Section 2.3),  $\kappa_\lambda$  is the continuous absorption coefficient and  $\tau_\lambda$  is the continuous optical depth at the wavelength  $\lambda_0$ .

We use Equation (2) and integrate over  $z$  instead of  $\tau_\lambda$  with the aid of  $d\tau_\lambda = \kappa_\lambda dz$  to find

$$r(\Delta\lambda) = \int_{-\infty}^{\infty} dz w(z) H\left(\frac{\lambda^2\gamma}{4\pi c\delta}, \frac{\Delta\lambda - \lambda_0\Phi(z)/c}{\delta}\right) \tag{4}$$

with

$$w(z) \equiv g_1(\tau_\lambda(z))\kappa(z)/\delta\sqrt{\pi}. \tag{5}$$

### 2.2. THE OBSERVED TIME- AND AREA-AVERAGED PROFILE

As derived in Equation (4),  $r(\Delta\lambda)$  is not yet related to an observable line profile. It must be averaged over the area  $A$  of the slit of the spectrograph, projected on the Sun

$$r(\Delta\lambda) = \int_{-\infty}^{\infty} dz w(z) \frac{1}{A} \iint_A dx dy H\left(\frac{\lambda^2\gamma}{4\pi c\delta}, \frac{\Delta\lambda - \lambda_0\Phi(z)/c}{\delta}\right). \tag{6}$$

This expression still contains all spatial and temporal dependences of  $\Phi$ ,  $\gamma$  and  $\delta$ . It fully describes the instantaneously observed profile of a weak line. If  $A$  is sufficiently large,  $r(\Delta\lambda)$  does not depend on  $t$  since nearly all possible values of  $\Phi(z)$  occur on  $A$  with the correct relative weight. A change in  $t$  amounts to a redistribution of the same set of values of the vertical velocity  $\Phi(z)$  over the area  $A$ , so the double integral in Equation (6) will have nearly always the same value. We formulate this more carefully: define a function  $f(z, v, t, A)dv$ =relative part of the area  $A$  at depth  $z$  where the line-of-sight component of the velocity field is between  $v$  and  $v+dv$ ; hence  $\int_{-\infty}^{\infty} dv f(z, v) = 1$ . Then, for any physical quantity  $G$  that depends on  $v$  only, one has

$$\frac{1}{A} \iint dx dy G(\Phi(x, y, z, t)) = \int_{-\infty}^{\infty} dv f(z, v, t, A) G(v). \tag{7}$$

For sufficiently large  $A$ ,  $f$  becomes independent of  $A$  and  $t$

$$\lim_{A \rightarrow \infty} f(z, v, t, A) = f(z, v).$$

Likewise Equation (6) is replaced by

$$r(\Delta\lambda) = \int_{-\infty}^{\infty} dz w(z) \int_{-\infty}^{\infty} dv f(z, v) H\left(\frac{\lambda^2\gamma}{4\pi c\delta}, \frac{\Delta\lambda - \lambda_0v/c}{\delta}\right). \tag{8}$$

This expression describes the line profile averaged over the observing time and the observed area. It is not linear, since  $\delta$  and  $\gamma$  are functions of  $T$  and  $P$ , hence of  $z$ ; they also depend on  $v$  insofar as correlations between  $v$  and  $T, P$  are present.

### 2.3. THE LINEARIZATION ASSUMPTIONS

We now make the critical assumptions that:

- (1)  $\delta$  and  $\gamma$  are not functions of  $v$ : then in Equation (8) the average value of  $\delta$  and  $\gamma$  over the surface at depth  $z$  can be used.
- (2) The lines are formed in a thin and homogeneous layer: i.e.,  $\delta$ ,  $\gamma$  and  $f$  are approximately constant over the layer of formation. It is then allowed to interpret  $\delta$ ,  $\gamma$  and  $f(v)$  as the Doppler width, damping constant, and the line of sight non-thermal velocity distribution at an *average* depth of line formation.

With these assumptions the integral over  $z$  in Equation (8) decouples

$$r(\Delta\lambda) = a \int_{-\infty}^{\infty} dv f(v) H\left(\frac{\lambda^2\gamma}{4\pi c\delta}, \frac{\Delta\lambda - \lambda_0 v/c}{\delta}\right), \quad (9a)$$

with

$$a = \int_{-\infty}^{\infty} dz w(z). \quad (9b)$$

We replace the integration variable  $v$  by  $x = \lambda v/c$  and introduce the following abbreviations

$$F(x) = \frac{c}{\lambda} f\left(\frac{c}{\lambda} x\right),$$

$$H(x) = H\left(\frac{\lambda^2\gamma}{4\pi c\delta}, \frac{x}{\delta}\right).$$

Equation (9a) is then shown to be a simple linear convolution integral

$$r(\Delta\lambda) = a \int_{-\infty}^{\infty} F(x) H(\Delta\lambda - x) dx \quad (10)$$

and the non-thermal velocity distribution  $F(x)$  can be found by deconvolution of the observed profile  $r(\Delta\lambda)$  with the known Voigt function  $H(x)$ , describing the broadening caused by damping and thermal motions only.

### 2.4. DECONVOLUTION

Since convolution is equivalent to multiplication in the Fourier transform domain, we obtain  $F(x)$  by dividing the Fourier transforms  $\tilde{r}(s)$  and  $\tilde{H}(s)$  of  $r(x)$  and  $H(x)$

$$\tilde{F}(s) = \tilde{r}(s)/a\tilde{H}(s), \quad (11)$$

and applying the inverse transform to the result. The advantages in this approach to deconvolution over previously used methods (e.g., De Jager and Neven, 1966) are the absence of any assumptions with regard to the shape and symmetry of the non-thermal

velocity distribution and the availability of the optimum noise filtering technique in the transform domain. The latter is especially important since the deconvolution process is very unstable. This is clear from Equation (11): the transform of a Voigt profile is given by (Bracewell, 1965 p. 357)

$$\tilde{H}(s) = \frac{1}{4\pi^2} \exp\left(-\left(\frac{\pi c}{\lambda^2} \delta s\right)^2 - \frac{\gamma}{2} |s|\right). \quad (12)$$

It decreases rapidly so that the high frequency terms in  $\tilde{r}(s)$  are greatly enhanced with respect to the low frequency terms. The deconvolution is only meaningful when  $\tilde{r}(s)$  decays faster than  $\tilde{H}(s)$  (or: when  $r(x)$  is wider than  $H(x)$ ). Since there is always some high frequency noise present in  $r(x)$  – if only caused by the finite sampling precision – the deconvoluted low frequency ‘signal’  $F(x)$  will be drowned completely in blown-up high frequency noise even when  $r(x)$  is much wider than  $H(x)$ . In the case that the noise and signal power spectra  $P_N(s)$  and  $P_S(s)$  of the observed line profile occupy quite different frequency bands, the obvious solution is multiplication in the Fourier transform domain with a properly chosen filter that passes only the signal band. In the more realistic case of overlapping signal and noise frequency bands but with random noise that is not correlated with the signal an ‘optimum’ filter is defined by (Helstrom, 1967; Brault and White, 1971)

$$\psi_{\text{opt}}(s) = \frac{P_S(s)}{P_S(s) + P_N(s)}. \quad (13)$$

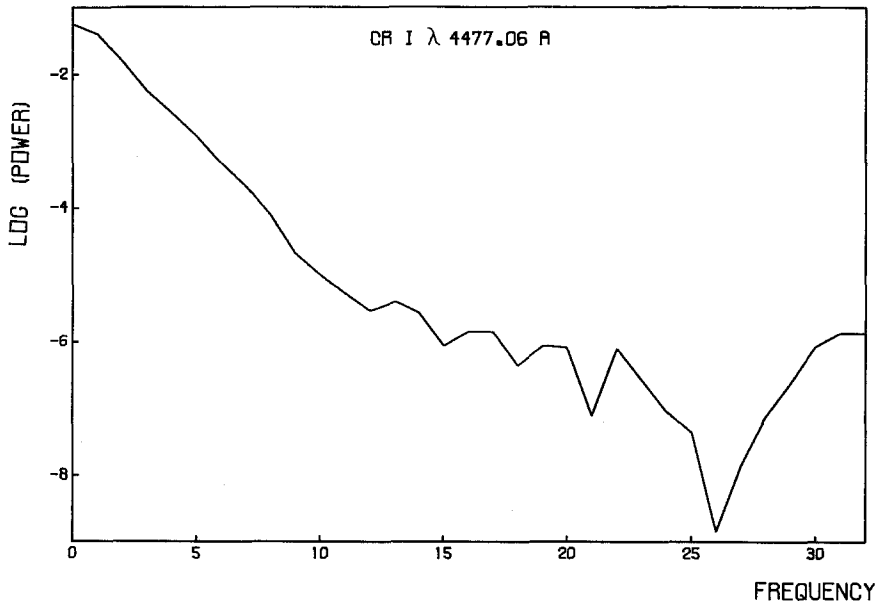


Fig. 1. Observed power spectrum, vertically:  $\log(|\tilde{r}(s)|^2)$  in arbitrary units; horizontally: frequency  $s$  in arbitrary units.

Of all possible linear shift invariant filters this filter gives the best approximation to the true  $F(x)$  in the rms sense. To use this filter, one has to know the power spectra  $P_S(s)$  and  $P_N(s)$  of the signal and noise components of the observed profile  $r(x)$  separately. To find these we plot the total raw power spectrum or 'periodogram' of  $r(x)$  on a logarithmic scale (Brault and White, 1971). A sample (Figure 1) shows that the signal and noise power spectra are clearly distinct: in general the signal has a steeply declining spectrum while the noise has a more or less constant spectrum. Since in the definition of the optimum filter  $\Psi_{\text{opt}}(s)$  only the frequency band where  $P_S(s) \simeq P_N(s)$  is important and the logarithmic signal power spectrum is nearly linear in this region, simple linear approximations to both  $\log P_S(s)$  and  $\log P_N(s)$  can be used.

### 2.5. AVERAGE DEPTH OF FORMATION

We need to know the damping and Doppler widths at the average depth of line formation. Gurtovenko *et al.* (1974) have shown that this depth must be determined from the line depression using the classical weighting function method that will be extended here to the whole profile of a weak line.

The equivalent width of a line is given by

$$A = \int w(z) \delta\sqrt{\pi} dz. \quad (14)$$

Assuming LTE we write (Unsöld, 1955, Equations (101), (50))

$$w(z) = g_1(\tau_\lambda) \kappa_{\text{tot}} / \delta\sqrt{\pi}, \quad (15)$$

with

$$g_1(\tau_\lambda) = \frac{\sec \vartheta}{\Phi^*(0)} \{ \Phi^*(\tau_\lambda) - B(\tau_\lambda) e^{-\tau_\lambda \sec \vartheta} \}, \quad (16)$$

$$\Phi^*(\tau_\lambda) = \int_{\tau_\lambda}^{\infty} B(\tau_\lambda) e^{-\tau_\lambda \sec \vartheta} d\tau_\lambda \sec \vartheta,$$

$$\kappa_{\text{tot}} = \frac{\pi e^2}{mc^2} \lambda^2 g_l f N(z). \quad (17)$$

In Equation (17)  $g_l$  is the statistical weight of the lower level of the transition,  $f$  the oscillator strength, and  $N(z)$  is the number density of the relevant particles in the lower level of the transition;  $N$  is computed assuming the validity of Saha's and Boltzmann's laws (LTE)

$$N(z) = N_{\text{tot}} \frac{N_{\text{element}}}{N_{\text{tot}}} \frac{N_r}{N_{\text{element}}} \frac{N_{r,s}}{N_r}, \quad \text{with } N_{\text{tot}} \sim P_g/T.$$

With Equations (14), (15) and (17) one obtains for the equivalent width of the line

$$A = \int g_1(\tau_\lambda) \kappa_{\text{tot}}(z) dz \sim \int g_1(\tau_\lambda) N(z) dz. \quad (18)$$

Hence the average optical depth of the whole line profile is

$$\langle \tau_\lambda \rangle = \frac{\int_0^\infty \tau_\lambda g_1(\tau_\lambda) N(\tau_\lambda) \frac{dz}{d\tau_\lambda} d\tau_\lambda}{\int_0^\infty g_1(\tau_\lambda) N(\tau_\lambda) \frac{dz}{d\tau_\lambda} d\tau_\lambda}, \quad (19)$$

where the weighting function  $g_1(\tau_\lambda)$  is conveniently written as

$$g_1 = \frac{\sec \vartheta}{\Phi^*(0)} \int_{\tau_\lambda}^\infty e^{-\tau_\lambda} \frac{dB}{d\tau_\lambda} d\tau_\lambda = \frac{\sec \vartheta}{\Phi^*(0)} \int_{B(\tau_\lambda)}^{B(\infty)} e^{-\tau_\lambda} dB. \quad (20)$$

### 3. Application to some Observed Line Profiles

#### 3.1. OBSERVATIONS

Through the kind cooperation of Dr L. Neven, Royal Observatory of Uccle-Brussels, and of Drs L. Delbouille and G. Roland, Astrophysical Institute of the Liège University, we obtained an accurate recording of a part of the solar spectrum observed in the disc center with the solar spectrograph at the Jungfrauoch Scientific Station. The observations were made in the 13th order; they cover the wavelength range from 4456 to 4477 Å, and are the result of 50 independent scans, averaged in the on-line computer. The recordings have an estimated scatter of 0.3% of the continuous spectrum intensity. See also the similar scans in Delbouille *et al.* (1973).

#### 3.2. SELECTION OF LINES

In this part of the spectrum a search was made for weak lines, i.e., lines that are still situated on the linear part of the curve of growth. From a standard empirical curve of growth (e.g., Unsöld, 1955, p. 444) it appears that such lines have an equivalent width  $W$  for which  $\log(W/\lambda) < -5.3$ , resulting at 4450 Å in a maximum value  $W = 22$  mÅ.

The lines to be selected should, furthermore, be unblended, while also their damping parameters should be known. Four lines appeared to suit these conditions; they are given in Table I. Their line profiles were read off plots of the the Jungfrauoch scans, to which continua and where necessary extensions of the line wings were fitted by hand. The apparatus profile is published in graphical form in Delbouille *et al.* (1973). At 4680 Å in the 13th order it has a full half width of 6 mÅ. This would correspond to a Doppler (half) half-width of 3.4 mÅ at 4460 Å or with an rms velocity of  $0.23 \text{ km s}^{-1}$ , which is negligibly small in the present rather qualitative test. The observed profiles were therefore *not* corrected for the influence of the apparatus profile.

TABLE I  
Lines used in this investigation

Atom $\lambda(\text{\AA})$	W (m $\text{\AA}$ )	Level designation { lower upper }	$g$	$\langle r^2 \rangle (\text{\AA})$		$gf$		$\chi_i$ (eV)
				Bates-Damgaard	Thomas-Fermi	Bates-Damgaard	Thomas-Fermi	
Cr I 4477.058	7	{ $3d^5(\alpha^4P)4s\alpha^2P_1$ $3d^5(\alpha^4P)4p\omega^5P_2^0$ }	3	29.8	30.6	0.000	0.000	2.71
				253	254			808
Cr I 4475.306	14	{ $3d^5(\alpha^6S)4pz^7P_2^0$ $3d^5(\alpha^6S)6sf^7S_3$ }	5	22.0	24.1	0.056	0	2.89
				384	387			8
Cr I 4460.778	13	{ $3d^5(\alpha^4F)4s\alpha^2P_2$ $3d^5(\alpha^4F)4p\omega^5P_2^0$ }	5	29.8	30.6	0.001	0.001	2.71
				257	258			88
V I 4452.007	22	{ $3d^4(\alpha^2H)4s\alpha^4H_{6,5}$ $3d^4(\alpha^2H)4pz^4I_{7,5^0}$ }	14	20.9	21.8	3.526		1.87
				89.8	92.0			3.858

### 3.3. AVERAGE OPTICAL DEPTH OF FORMATION

These values were computed according to Equation (19) using the Harvard Smithsonian Reference Atmosphere (Gingerich *et al.*, 1971). The resulting  $\langle \tau_0 \rangle$  values are given in Table II. The part of the photosphere that contributes to the line depression is rather wide: see Figure 2. Also the average optical depth computed via a computation of the

TABLE II  
Damping parameters for the level of the average optical depth of formation

Atom	$\lambda(\text{\AA})$	$\langle \tau_0 \rangle$	$T(\text{K})$	$2.7\gamma (\text{s}^{-1})$
Cr I	4477.06	0.50	5890	$1.18 \times 10^{10}$
Cr I	4475.31	0.53	5920	$1.37 \times 10^{10}$
Cr I	4460.78	0.50	5890	$1.18 \times 10^{10}$
V I	4452.01	0.39	5760	$6.72 \times 10^9$

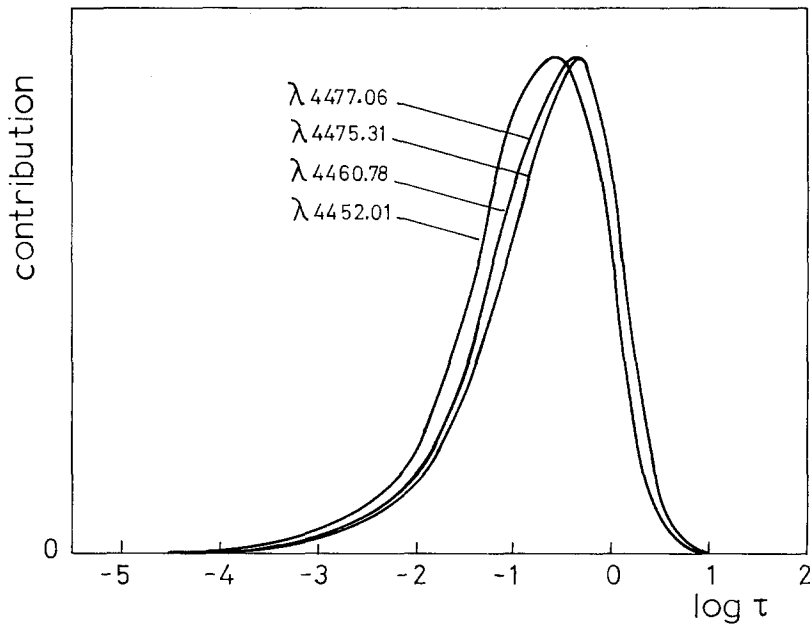


Fig. 2. Contribution functions of the four investigated lines.

average *geometrical* depth differs from the values of Table II. For the Cr I line at 4477 Å:  $\langle z \rangle = -97$  km, ( $z=0$  at  $\tau_5=1$ ) which corresponds to a  $\tau_5$ -value of 0.19 (cf.:  $\langle \tau_5 \rangle = 0.50$ ). This difference is due to the non-linearity of the relation between  $\tau_0$  and  $z$ , and to the skewness of the contribution function, and makes it clear that the notion 'average optical depth' has only an indicative value and should surely not be considered as a precise indicator of the level of origin of the lines.

The weakness of the lines was checked by using a spectral line synthesis program (Wijbenga and Zwaan, 1972) to calculate the emergent profiles including microturbulence ( $1.5 \text{ km s}^{-1}$ ) and depth-dependent damping.

For each line we fitted the abundance to the observed equivalent width and then computed the equivalent width using half this abundance. The results show that the lines are indeed on the linear part of the curve of growth, except for V I  $\lambda 4552.01$  that already shows slight self-absorption.

### 3.4. DAMPING PARAMETERS

Even for these weak lines damping cannot be completely neglected. The damping is the combined effect of the influences of Van der Waals broadening, quadrupole interaction and the quadratic Stark effect due to electronic collisions (in this succession of importance). Their values ( $\gamma$ ) were computed according to De Jager and Neven (1970).

The necessary values of the radial wave functions  $r$ , the mean square radii  $\langle r^2 \rangle$  for the atomic states, and the oscillator strengths were at our request kindly computed by Dr W. van Rensbergen of the Astrophysical Institute of the Free University of Brussels, according to a method applied earlier by him to other lines (Van Rensbergen, 1970). The results are given in Table I, the computations according to the 'scaled Thomas-Fermi method' are considered to be the more reliable ones and were used in the following computations. Damping constants were computed for the four lines for the physical parameters ( $T, P_g, P_e$ ) read from the Harvard-Smithsonian Reference Atmosphere at the average depths of formation given in Table II. For their practical application we used the empirical result of De Jager and Neven (1970) that the actual values for the damping parameters seem to be about 2.7 times the theoretical values computed on the basis of  $\langle r^2 \rangle$  values found with the 'scaled Thomas-Fermi method'. An empirical correction of similar value was found by Holweger (1972). It should, however, be remarked that its value is not very critical since the influence of damping on the results is small anyhow.

The resulting  $\gamma$ -values are given in Table II.

### 3.5. FOURIER TRANSFORM

We used the ALGOL'60 Fast Fourier Transform procedures given by Singleton (1968) and applied the recipes given by Brault and White (1971) to ensure a clean transform. The Voigt profiles were calculated with the series expansions given by Reichel (1968).

The effect of the filtering on the original observations is shown in Figure 3 where the observed profile is given with the approximation to it obtained with the optimum filter in the transform domain; the lost high frequencies clearly convey no spectral information. The quality of the optimum filter, described in Section 2.4, is clear from Figure 4 in which instead of the optimum filter a simple filter has been used that has an unsmoothed steplike cut-off, introducing strong oscillations. Figure 5 shows the same velocity distribution but obtained with the optimum filter.

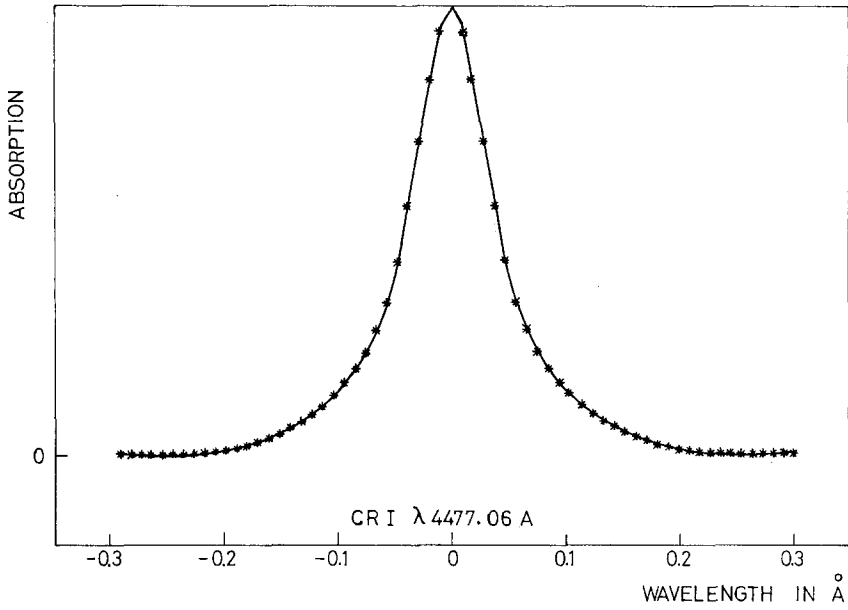


Fig. 3. Observed profile (full drawn line) and filtered approximation to it (crosses).

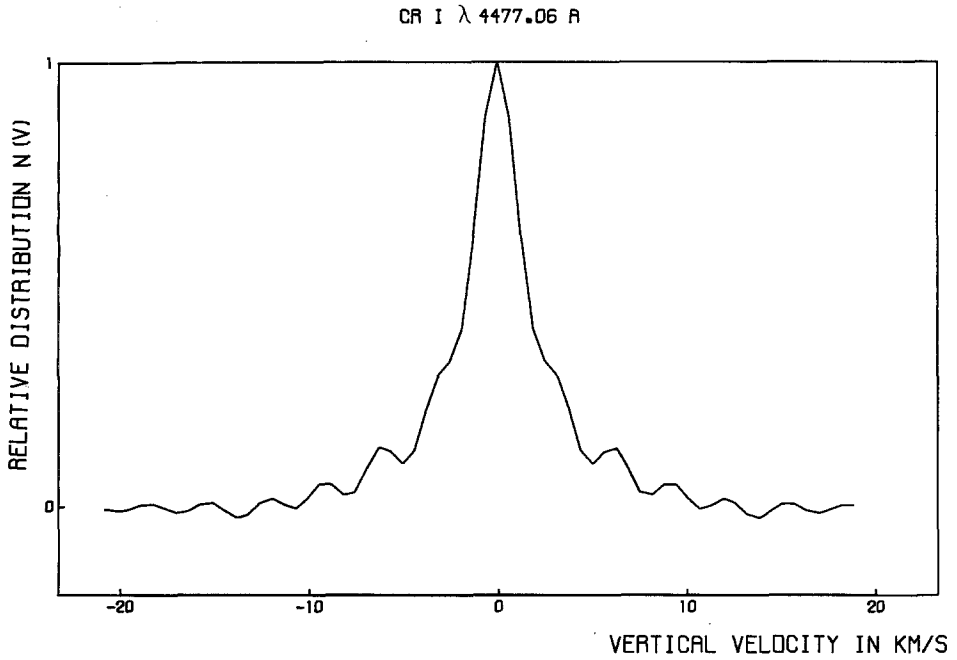


Fig. 4. Velocity distribution obtained with a simple cut-off filter.

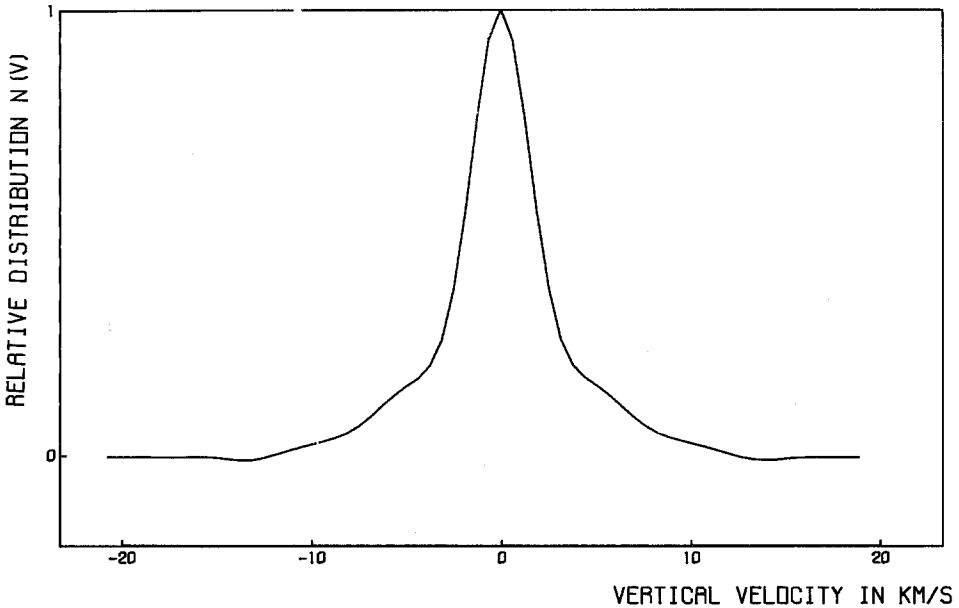


Fig. 5. Velocity distribution obtained with the optimum filter.

#### 4. Results

In view of the usual uncertainties in  $gf$ ,  $A$  etc. we did not evaluate the constant  $a$  in Equation (10) so that the four line profiles yield relative distribution functions; these are shown in Figure 6. The rms velocities, calculated from the observed profiles with

$$\langle v^2 \rangle^{1/2} = \frac{c}{\lambda} ((\Delta\lambda^2)_{\text{observed}} - (\Delta\lambda^2)_{\text{Voigt}})^{1/2}$$

with

$$(\Delta\lambda^2)_{\text{Voigt}} = \frac{\delta^2}{2} + \frac{\gamma^2 \lambda^4}{16\pi^2 c^2}$$

are given in Table III, together with the rms velocity of a gaussian with the same half-width as the distributions, found from

$$\langle v^2 \rangle_{\text{Gauss}}^{1/2} = 0.425 * FHW(f(v)).$$

The resulting rms velocity values range between 2 and 4 km s<sup>-1</sup> and agree in general with the quadratic sum of quoted micro- and macroturbulent velocities (De Jager, 1972). All distributions are wider than gaussians; however, the spread in the shapes of the distribution functions is large. All four lines are formed at about the same level in the atmosphere, so they should show similar velocity broadening; since they do not, we must question the validity of the two linearization assumptions made in Section

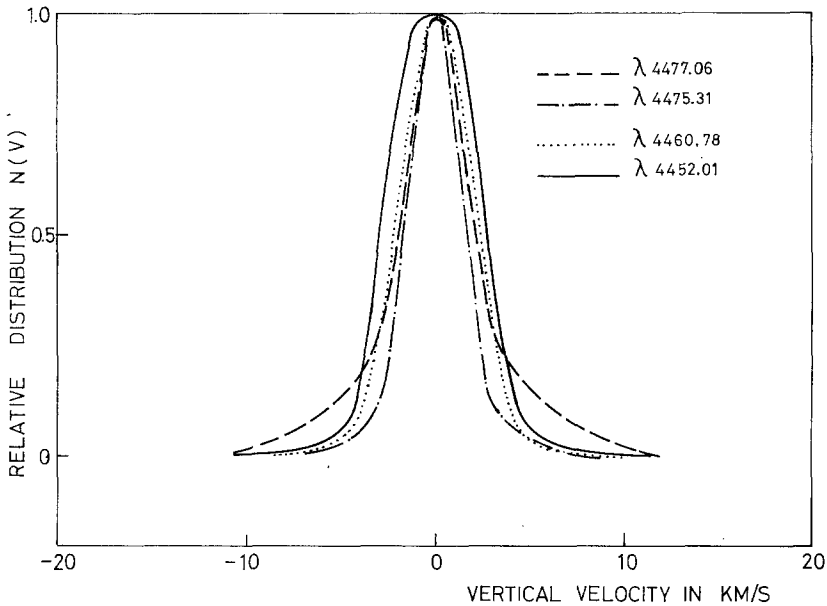


Fig. 6. Velocity distributions for the four investigated lines.

TABLE III  
rms velocity values

Atom	$\lambda(\text{\AA})$	$\langle v^2 \rangle^{1/2}$ ( $\text{km s}^{-1}$ )	$\langle v^2 \rangle^{1/2}_{\text{gauss}}$ ( $\text{km s}^{-1}$ )	$\langle v^2 \rangle^{1/2}_{\text{theoretical}}$ ( $\text{km s}^{-1}$ )
Cr I	4477.06	3.7	1.8	2.4
Cr I	4475.31	2.3	1.5	2.1
Cr I	4460.78	2.6	1.4	1.7
V I	4452.01	2.6	2.4	2.8

2.3. Of course, errors in the determination of the continuum level or the calculation of the depth of formation and  $\gamma$  also influence the results; these errors might be reduced by using a large number of profiles, all originating at about the same depth.

With regard to the linearization assumptions, it is difficult to see that the second assumption (stating that the lines are formed in a layer thin enough to be homogeneous) causes this diversity, since the contribution functions of these lines are not very different from each other. The first assumption ( $\delta$  and  $\gamma$  are independent of  $v$ ) is the most critical one. If it is not correct, studies of the solar motion field must be multidimensional.

Usually gaussians are taken for both micro- and macroturbulent distribution functions, and usually these are convoluted under the first assumption, respectively with the absorption coefficient and the emergent profile. We note that next to the indication that the first assumption is perhaps incorrect, the four derived distribution functions are not gaussian but have significantly extended wings. Again, a further analysis of a

larger number of profiles is needed to confirm this behaviour. An obvious extension will then be to study center-to-limb and depth behaviour of the velocity distribution.

In conclusion the analysis of these four lines shows that the method presented here is suitable to find the average velocity distribution when the linearization assumptions (that are implicitly made in many analyses) hold, but does not present a clear affirmation of these assumptions. Also a wider than Gaussian velocity is indicated, with a rms velocity of about  $3 \text{ km s}^{-1}$ .

#### 4.1. COMPARISON WITH THEORETICAL VELOCITY DISTRIBUTIONS

De Jager (1974) published theoretical profiles of weak Fraunhofer lines in the absence of damping and thermal broadening that were calculated from assumed spectra of turbulence, characterized by a power law  $k^{-n}$ , yielding Kolmogoroff's law for  $n = \frac{2}{3}$ .

He calculated theoretical profiles both with and without variation of the largest turbulent wavelength, which was estimated from granulation cell statistics; samples are given in Figure 7.

These theoretical distribution functions are quite different from the ones found in the above analysis: they are all doubly peaked. However, the distribution functions found by deconvolution are not unique: there is a multitude of mathematically correct solutions containing different high frequency contributions. We therefore tested the compatibility of De Jager's distributions with the four observed profiles the other way

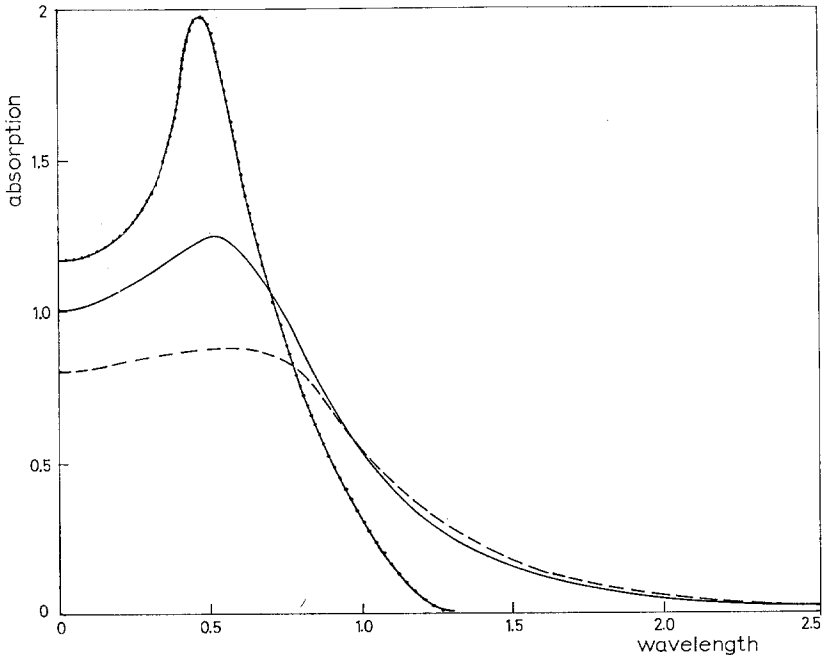


Fig. 7. Theoretical weak line profiles broadened by turbulence only, taken from De Jager (1974). Top curve:  $n = 2$ ; middle curve:  $n = 2/3$ ; bottom curve (dashed):  $n = 2/3$  but with granulation size distribution included.

around by convoluting them with the Voigt profiles determined by damping and thermal motions, varying the width of the distribution to obtain maximum fit between the result and the observed profiles. In this procedure again the linearization assumptions of Section 2.3 are made.

The results show that the double-peak feature is wholly lost and that the observed profiles are quite well reproduced by the convoluted distribution, except for the wings which are more extended in some observed profiles (Figure 8). The differences be-

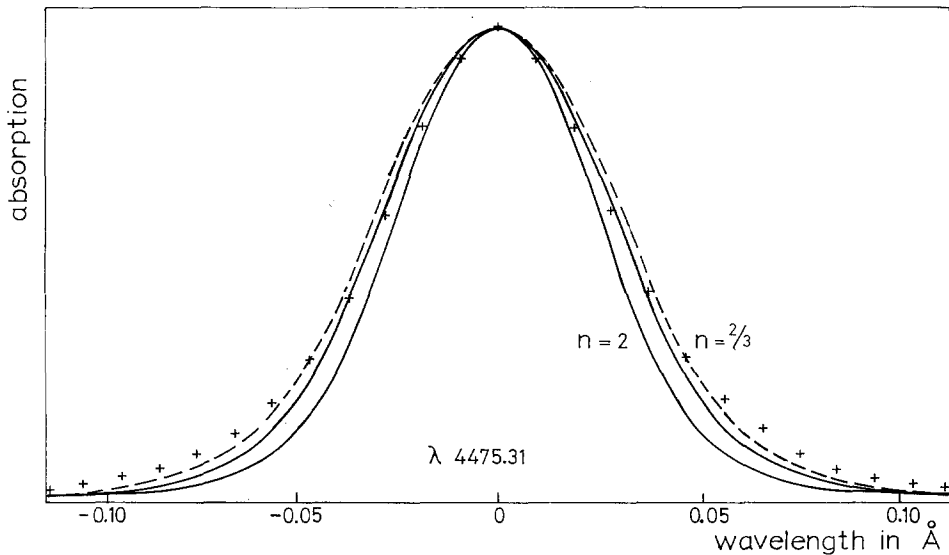


Fig. 8. Line profiles resulting from the convolution of the theoretical turbulence profile with thermal motions and damping. Crosses: observed profile. Dashed: granulation cell size included.

tween the distribution without and with granulation cell variation are too small to warrant a choice; the distributions with  $n=2/3$  fit better than those with larger  $n$  since they have more extended wings. The fitted distribution width finally determines the mean turbulent velocity: in Table III we give the rms values. Most of these are smaller than the rms velocities found in the preceding analysis, corresponding to the lack of wing in the convoluted profiles. From these four lines we conclude that the theoretical distributions are not incompatible with the observations, with an indication that the turbulent energy spectrum is Kolmogoroffian.

#### Acknowledgements

We are indebted to Dr L. Neven for the Jungfrauoch observations, to Drs J. T. Jefferies and C. Zwaan for critical discussions, to Dr J. Houtgast for comments on the manuscript and to Mr G. W. Geijtenbeek for assistance with the programming.

### References

- Bracewell, R.: 1965, *The Fourier Transform and Its Applications*, McGraw-Hill, New York.
- Brault, J. W. and White, O. R.: 1971, *Astron. Astrophys.* **13**, 16.
- Cooley, J. W. and Tukey, J. W.: 1965, *Math. Comput.* **19**, 297.
- De Jager, C.: 1972, *Solar Phys.* **25**, 71.
- De Jager, C.: 1974, *Solar Phys.* **34**, 91.
- De Jager, C. and Neven, L.: 1966, *Bull. Astron. Inst. Neth.* **18**, 336.
- De Jager, C. and Neven, L.: 1970, *Solar Phys.* **11**, 3.
- Delbouille, L., Roland, G., and Neven, L.: 1973, *Photometric Atlas of the Solar Spectrum from  $\lambda$ 3000 to  $\lambda$ 10000*. Published by Institut d'Astrophysique de l'Université de Liège.
- Gingerich, O., Noyes, R. W., Kalkoven, W., and Cuny, Y.: 1971, *Solar Phys.* **18**, 347.
- Gurtovenko, E., Ratnikova, V., and De Jager, C.: 1974, *Solar Phys.* **37**, 43.
- Helstrom, C. W.: 1967, *J. Opt. Soc. Am.* **57**, 297.
- Holweger, H.: 1972, *Solar Phys.* **25**, 14.
- Reichel, A.: 1968, *J. Quant. Spectrosc. Radiat. Transfer* **8**, 1601.
- Singleton, R. C.: 1968, *Comm. ACM* **11**, 773.
- Unsöld, A. 1955, *Physik der Sternatmosphären*, 2. Aufl., Springer, Berlin.
- Van Rensbergen, W.: 1970, *Solar Phys.* **11**, 11.
- Wijbenga, J. W. and Zwaan, C.: 1972, *Solar Phys.* **23**, 265.